

# Timelike Compton scattering off the neutron

M. Boër<sup>1</sup>, M. Guidal<sup>1</sup> and M. Vanderhaeghen<sup>2</sup>

<sup>1</sup>*Institut de Physique Nucléaire d'Orsay, CNRS-IN2P3, Université Paris-Sud, Université Paris-Saclay, 91406 Orsay, France*

<sup>2</sup>*Institut für Kernphysik and PRISMA Cluster of Excellence, Johannes Gutenberg Universität, Mainz, Germany.*

We study the exclusive photoproduction of an electron-positron pair on a neutron target in the Jefferson Lab energy domain. The reaction consists of two processes: the Bethe-Heitler and the Timelike Compton Scattering. The latter process provides potentially access to the Generalized Parton Distributions (GPDs) of the nucleon. We calculate all the unpolarized, single- and double-spin observables of the reaction and study their sensitivities to GPDs.

PACS numbers:

## I. INTRODUCTION

In a recent article [1], we studied the exclusive photoproduction of an electron-positron pair off a proton target, i.e. the  $\gamma p \rightarrow p' e^+ e^-$  reaction, in the multi-GeV beam energy domain. For sufficiently large invariant masses of the final lepton pair  $Q'^2 = (e^+ + e^-)^2 \gtrsim 4 \text{ GeV}^2$  and small squared nucleon momentum transfer  $-t = -(p' - p)^2 \lesssim 1 \text{ GeV}^2$ , the process allows to study the partonic substructure of the proton. In particular, it provides access to the Generalized Parton Distributions (GPD) of the proton. We refer the reader to Refs. [2–6] for reviews and details on the GPD concepts and formalism. In simple terms, the GPDs are universal structure functions which allow to map the correlated transverse position-longitudinal momentum distributions of the quarks and gluons within the nucleon. These correlations are up to now barely known. In Ref. [1], we calculated, in addition to the unpolarized cross sections, all the single- and double-spin beam/target observables of the  $\gamma p \rightarrow p' e^+ e^-$ . We showed their sensitivities to the different GPDs. In this article, we extend this work to a neutron target with the aim of studying the sensitivity of the process to neutron GPDs.

The  $\gamma N \rightarrow N' e^+ e^-$  reaction (where  $N$  stands for a proton  $p$  or a neutron  $n$ ) consists of two processes: the Bethe-Heitler (BH) and the Timelike Compton Process (or TCS for Timelike Compton Scattering). See Fig. 1 for a sketch of the two processes. In the BH process, the final state lepton pair originates directly from the initial photon of the beam which is a pure QED (Quantum Electro-Dynamics) process. One of the leptons interacts then with the nucleon through the exchange of a virtual spacelike photon. This process involves the elastic form factors of the nucleon. These are rather accurately known in the low nucleon momentum transfer  $t$  region that concerns us. The whole process is therefore quite precisely calculable. In the TCS process, the final state lepton pair originates from the timelike virtual photon which, if its virtuality  $Q'^2$  is high enough, is emitted off a quark from the target nucleon. Therefore, the final lepton pair kinematic distribution can be expected to reflect some aspects of the intrinsic dynamics and interactions

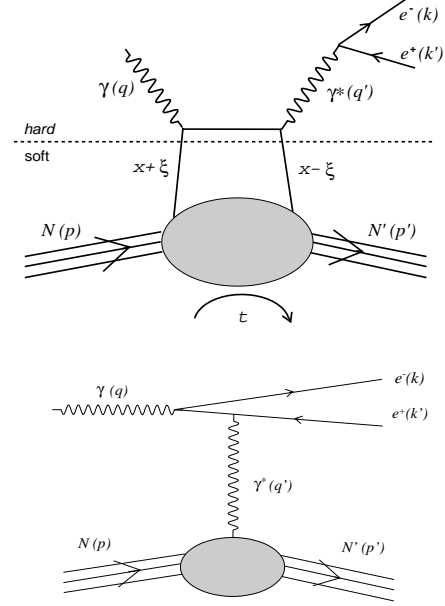


Figure 1: Top: The direct TCS diagram (at QCD leading-twist); there is also a crossed diagram. Bottom: The BH diagram; there is also a diagram where the spacelike virtual photon couples to the electron instead of the positron.

of the quarks in the nucleon. It can be shown in Quantum Chromo-Dynamics (QCD) that, at low  $t$  and large  $Q'^2$ , there is a factorization between the hard elementary Compton scattering at the quark level and the universal structure functions called GPDs [8–11]. These functions encompass the complex quark and gluon structure of the nucleon, which cannot be calculated at this time from the first principles of QCD.

There are, at QCD leading twist, 4 chiral even nucleon GPDs entering the TCS process, :  $H$ ,  $E$ ,  $\tilde{H}$  and  $\tilde{E}$ . They reflect the four independent quark helicity-nucleon spin transitions between the initial and final states. Neglecting QCD evolution effects, which is the farmework of this work, the GPDs depend on three kinematic vari-

ables  $x, \xi, t$ . In a frame where the nucleon approaches the speed of light,  $x$  and  $\xi$  define the initial and final quark longitudinal momentum fractions ( $x + \xi$  and  $x - \xi$  respectively, see Fig. 1). The GPDs can then be interpreted as the probability amplitude to find a quark in the initial (final) nucleon with a longitudinal momentum fraction  $x + \xi$  ( $x - \xi$ ). In addition, the process involves a small transverse momentum transfer which is contained in  $t$ . At  $\xi = 0$ , GPDs provide access to the probability amplitude to find a quark in the nucleon with a *longitudinal* momentum fraction  $x$  at a given *transverse* impact parameter  $b_\perp$ , which is the conjugate variable of  $t$ .

This article is organized as follows. After a brief review of the formalism in section II, we show the results of our calculations for different observables in section III and present our conclusions in section III.

## II. FORMALISM

We presented in Ref. [1] the formalism that we used to derive the amplitudes of the BH and TCS processes on the proton. We now make a brief recap, which we adapt to the neutron target case.

We use a frame where the average photons momenta  $\bar{q} = \frac{1}{2}(q + q')$  and neutrons momenta  $N = \frac{1}{2}(p + p')$  are collinear along the  $z$ -axis and in opposite directions. We define the lightlike vectors along the positive and negative  $z$  directions as:

$$\tilde{p}^\mu = P^+/\sqrt{2}(1, 0, 0, 1), \quad (1)$$

$$n^\mu = 1/\sqrt{2}P^+(1, 0, 0, -1), \quad (2)$$

where the light-cone components  $a^\pm$  are defined by  $a^\pm \equiv (a^0 \pm a^3)/\sqrt{2}$ .

In this frame, using Ji's conventions for the GPDs [10, 11], the TCS amplitude reads:

$$\begin{aligned} T^{TCS} = & -\frac{e^3}{q'^2} \bar{u}(k) \gamma^\nu v(k') \epsilon^\mu(q) \\ & \times \left\{ \frac{1}{2} (-g_{\mu\nu})_\perp \int_{-1}^1 dx \left( \frac{1}{x - \xi - i\epsilon} + \frac{1}{x + \xi + i\epsilon} \right) \right. \\ & \times \left( H^n(x, \xi, t) \bar{u}(p') \not{n} u(p) \right. \\ & \left. + E^n(x, \xi, t) \bar{u}(p') i\sigma^{\alpha\beta} n_\alpha \frac{\Delta_\beta}{2m} u(p) \right) \\ & - \frac{i}{2} (\epsilon_{\nu\mu})_\perp \int_{-1}^1 dx \left( \frac{1}{x - \xi - i\epsilon} - \frac{1}{x + \xi + i\epsilon} \right) \\ & \times \left( \tilde{H}^n(x, \xi, t) \bar{u}(p') \not{n} \gamma_5 u(p) \right. \\ & \left. + \tilde{E}^n(x, \xi, t) \bar{u}(p') \gamma_5 \frac{\Delta \cdot n}{2m} u(p) \right) \left. \right\}, \end{aligned} \quad (3)$$

where we have used the metrics:

$$\begin{aligned} (-g_{\mu\nu})_\perp &= -g_{\mu\nu} + \tilde{p}_\mu n_\nu + \tilde{p}_\nu n_\mu, \\ (\epsilon_{\nu\mu})_\perp &= \epsilon_{\nu\mu\alpha\beta} n^\alpha \tilde{p}^\beta. \end{aligned} \quad (4)$$

In Eq. 3,  $m$  is the neutron mass and the light-cone momentum fractions  $x$  and  $\xi$  are defined respectively by  $k^+ = xP^+$ , and by  $\Delta^+ = -2\xi P^+$  where  $\Delta^\mu = (p' - p)^\mu = (q - q')^\mu$ . We have  $\xi = \frac{Q'^2}{2(s - m^2) - Q'^2}$ , where  $s = (p + q)^2$ , when we neglect  $\Delta$  terms w.r.t. to  $Q'^2$ . In the following, we will place ourselves in this limit. In Ref. [1], we compared this limit with the exact kinematics and formulae and we found that the effects on the observables associated to this approximation were negligible for the Jefferson Lab (JLab) kinematics discussed in the following. Regarding the GPDs, for numerical estimates, we will use the parameterization given by the VGG model [2, 7, 12, 13]. The  $x, \xi$ -dependence follows the double-distribution ansatz [8, 14, 15] and the  $t$ -dependence is Reggeized [2, 7]. The VGG model contains also the so-called D-term [16] whose influence will be studied in the following.

GPDs are defined for each quark flavor. Restricting ourselves to the  $u$  and  $d$  flavors, we have the following decomposition for the neutron and the proton:

$$GPD^n(x, \xi, t) = \frac{1}{9} GPD^u + \frac{4}{9} GPD^d, \quad (5)$$

$$GPD^p(x, \xi, t) = \frac{4}{9} GPD^u + \frac{1}{9} GPD^d.$$

The simultaneous study of TCS off the proton and off the neutron therefore allows to make a flavor separation of GPDs.

The BH amplitude reads:

$$\begin{aligned} T^{BH} = & -\frac{e^3}{\Delta^2} \bar{u}(p') \Gamma^\nu u(p) \epsilon^\mu(q) \\ & \times \bar{u}(k) \left( \gamma_\mu \frac{\not{k} - \not{q}}{(k - q)^2} \gamma_\nu + \gamma_\nu \frac{\not{q} - \not{k}'}{(q - k')^2} \gamma_\mu \right) v(k'), \end{aligned} \quad (6)$$

with the virtual photon-neutron electromagnetic vertex matrix

$$\Gamma^\nu = \gamma^\nu F_1^n(t) + \frac{i\sigma^{\nu\rho} \Delta_\rho}{2m} F_2^n(t). \quad (7)$$

$F_1^n(t)$  and  $F_2^n(t)$  are the neutron Dirac and Pauli form factors. In this work, we take the parametrizations based on Refs. [17, 18].

At fixed beam energy  $E_\gamma$  or longitudinal momentum transfer fraction  $\xi$ , there are four independent kinematical variables for the process  $\gamma N \rightarrow N' e^+ e^-$ . We choose them as:  $Q'^2$  and  $t (= \Delta^2)$  that we already defined, and the two angles  $\theta$  and  $\phi$  of the electron in the leptons' center-of-mass frame. The polar angle  $\theta$  is defined w.r.t. to the  $z'$ -axis which correspond to the direction of the two-lepton system in the  $(e^+ e^-) - N'$  center of mass and  $\phi$  is the azimuthal angle between the decay plane and the production plane. We refer the reader to Fig.4 of Ref. [1] for an illustration and the orientation of the angles.

### III. CALCULATION OF OBSERVABLES

#### A. Unpolarized cross section

The 4-fold differential unpolarized cross section is expressed as:

$$\frac{d^4\sigma}{dQ'^2 dt d\Omega}(\gamma N \rightarrow Ne^+e^-) = \frac{1}{2\pi^4} \frac{1}{64} \frac{1}{2mE_\gamma} \quad (8)$$

$$\times |T^{BH} + T^{TCS}|^2$$

where  $T^{BH} + T^{TCS}$  is summed over the final nucleon and final electron helicities and is averaged over the target nucleon helicities and beam polarizations.

We present in Fig. 2 the results of our calculations for the  $t$ -dependence of the two-fold unpolarized TCS and BH cross sections  $\frac{d\sigma}{dQ'^2 dt}$ . The calculations have been performed at  $\xi = 0.2$  and  $Q'^2 = 7 \text{ GeV}^2$ , which is a typical kinematical setting accessed at JLab 12 GeV. The angles  $\theta$  and  $\phi$  have been integrated over  $[\pi/4, 3\pi/4]$  and  $[0, 2\pi]$  respectively. The general motivation for integrating over  $\theta$ , which we will do for all observables in the following, is to maximize the count rates from an experimental point of view. We showed in Ref. [1] that this did not result in an important loss of sensitivity to TCS, and therefore to GPDs, compared to a fixed  $\theta$  value. The reason for limiting the range of integration in  $\theta$  is that the BH exhibits (quasi-)singularities around  $\theta=0^\circ$  ( $\theta=180^\circ$ ). These regions correspond to cases where the electron (positron) is emitted in the direction of the initial photon, so that the lepton propagator becomes singular and creates a sharp peak in the cross section. In order to optimize the sensitivity to TCS, it is therefore advisable to keep away from the BH-dominated regions such as  $\theta=0^\circ$  ( $\theta=180^\circ$ ).

In Fig. 2, we compare  $\frac{d\sigma}{dQ'^2 dt}$  for the neutron and proton target cases. For both, the BH cross section is more than one order of magnitude higher than the TCS one. As a consequence, as we discussed in Ref. [1], the sensitivity to TCS, and thus to GPDs, will better show up through interference effects, and therefore spin observables. Both the BH and TCS neutron cross sections are less than a factor of two lower than the corresponding proton cross sections. The neutron channel is therefore in principle measurable experimentally, modulo neutron detection efficiency issues. We recall that a proposal for measuring TCS on the proton at JLab has already been approved [19]. We also display in Fig. 2 the neutron BH cross section calculated with only the neutron magnetic form factor contribution. This curve is almost indistinguishable from the calculation with both form factors, which shows that the neutron BH cross section is largely dominated by the contribution of the neutron magnetic form factor.

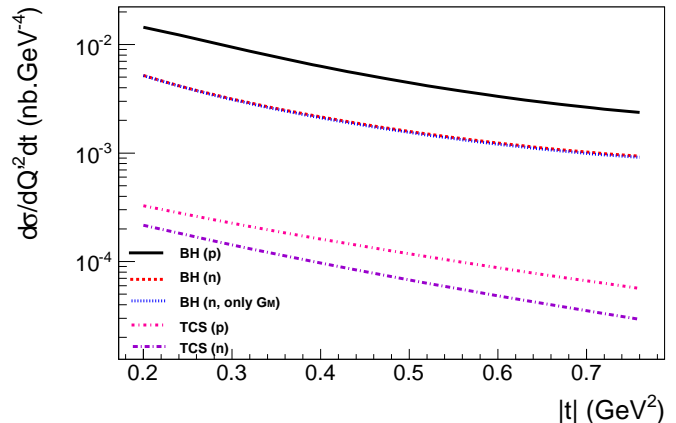


Figure 2: Unpolarized cross sections  $\frac{d\sigma_{BH}}{dQ'^2 dt}$  for BH and for TCS off the neutron and proton. The calculations have been done at  $\xi = 0.2$  and  $Q'^2 = 7 \text{ GeV}^2$ . The angles  $\theta$  and  $\phi$  have been integrated over  $[\pi/4, 3\pi/4]$  and  $[0, 2\pi]$  respectively. The neutron BH calculation with only the neutron magnetic form factor contribution is also shown.

#### B. Single spin asymmetries

In this section, as well as in the following one on double spin asymmetries, our calculations are carried out for 100% polarisation. Circularly polarized photons, linearly polarized photons and polarized targets with high degrees of polarization (between 60% and 90%) have been obtained and used these past years almost routinely at JLab (see for instance Ref. [20]).

Following the conventions of Ref. [1], we use the notation  $A_{ij}$  for the spin asymmetries where the first index refers to the polarization of the beam and the second one to the polarization of the target. There are three sorts of single-spin asymmetries:

$$A_{\odot U} = \frac{\sigma^+ - \sigma^-}{\sigma^+ + \sigma^-}, \quad (9)$$

$$A_{\ell U}(\Psi) = \frac{\sigma(\Psi) - \sigma(\Psi + \pi/2)}{\sigma(\Psi) + \sigma(\Psi + \pi/2)}, \quad (10)$$

$$A_{Ui} = \frac{\sigma^+ - \sigma^-}{\sigma^+ + \sigma^-}. \quad (11)$$

They are associated respectively to a circular polarized beam, a linearly polarized beam and a polarized target. The index  $U$  stands for “unpolarized”. For the target spin asymmetries  $A_{Ui}$ , the index  $i = x, y, z$  corresponds to the polarization direction of the target along the  $x, y, z$  axis respectively. The  $z$ -axis is along the photon direction in the  $\gamma - N$  center of mass system, the  $y$ -

axis is perpendicular to the reaction plane and the  $x$ -axis is perpendicular to the target nucleon direction and in the reaction plane (see Fig.4 of Ref. [1] for an illustration of our axis orientation convention). The superscripts  $\pm$  refer to the target spin orientation along those axis. For the circularly polarized asymmetry  $A_{\ell U}$ ,  $\Psi$  is the angle between the polarization vector of the incoming photon and the scattering plane. For the linearly polarized asymmetry  $A_{\odot U}$ , the  $+$  superscript refers to the right circular polarization and the  $-$  superscript to the left circular polarization.

We begin by studying the linearly polarized beam single-spin asymmetry. Similarly to the proton target case,  $A_{\ell U}$  shows a typical  $\cos(2\Psi)$ -like modulation which we do not show here. In the following, we therefore calculate  $A_{\ell U}$  for  $\Psi = 0^\circ$ . The upper panel of Fig. 3 shows the  $\phi$ -dependence of  $A_{\ell U}$  for the  $\gamma n \rightarrow n'e^+e^-$  reaction for  $\Psi = 0^\circ$ ,  $\xi = 0.2$ ,  $Q'^2 = 7 \text{ GeV}^2$ ,  $-t = 0.4 \text{ GeV}^2$  and  $\theta$  integrated over  $[\pi/4, 3\pi/4]$ . This observable is sensitive to the real part of the BH + TCS amplitude. We recall that the BH amplitude is purely real. It is seen in Fig. 3 that the BH alone produces actually most of the signal, with an amplitude around 30%. The TCS, essentially through the GPD  $H^n$ , brings only small variations around  $\phi = 90^\circ$  w.r.t. the BH signal. The introduction of the  $\tilde{H}^n$ ,  $E^n$  and  $\bar{E}^n$  GPDs barely changes the asymmetry calculated with only  $H$ . However, the introduction of the D-term is noticeable. In the bottom panel of Fig. 3, we show the  $t$ -dependence of  $A_{\ell U}$  for  $\phi = 90^\circ$  for both the neutron and proton cases (this latter asymmetry was calculated in Ref. [1]). The amplitude of both asymmetries increases with  $|t|$ , faster for the neutron than for the proton. In both cases, the TCS contribution diminishes the amplitude of the asymmetry. The sensitivity of the asymmetry to the GPDs grows with increasing values of  $|t|$ , with a dominating influence of  $H^n$  and of the D-term.

In Fig. 4, we show the other beam single-spin asymmetry  $A_{\odot U}$ , i.e. obtained with a circularly polarized photon beam. Like for the proton case [1], the asymmetry exhibits for the  $\gamma n \rightarrow n'e^+e^-$  reaction a  $\sin \phi$ -like shape and we display in Fig. 4  $A_{\odot U}$  as a function of  $t$  for  $\phi = 90^\circ$  (at  $\xi = 0.2$ ,  $Q'^2 = 7 \text{ GeV}^2$  and  $\theta$  integrated over  $[\pi/4, 3\pi/4]$ ). One notices that the BH alone produces a zero asymmetry. This is due to the fact that the  $A_{\odot U}$  observable is sensitive to the imaginary part of the amplitude, making this observable very favorable for the study of TCS and GPDs. When the TCS process is included, the asymmetries on the neutron target reach up to 5% at the largest values of  $|t|$  considered here. From Fig. 4, one sees that this observable has a sensitivity to  $H^n$  but also to  $\tilde{H}^n$  and  $E^n$ . It is particularly interesting to note that when only  $H^n$  is taken into account,  $A_{\odot U}$  for the neutron case is positive while it becomes negative when  $E^n$  is introduced. The explanation is the following. The asymmetry results from the interference of the BH and TCS processes. It is therefore proportional to the product of the two amplitudes. As

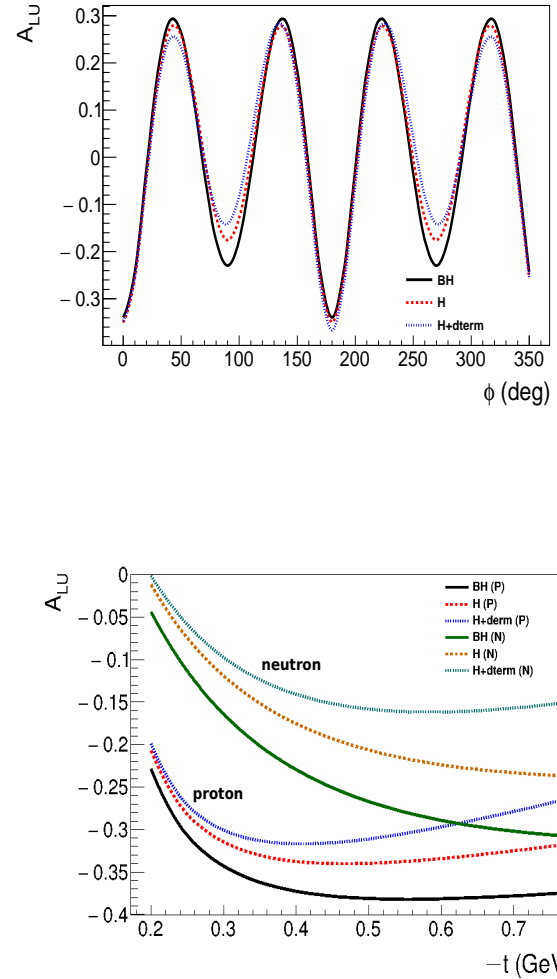


Figure 3: Top panel:  $A_{\ell U}$  as a function of  $\phi$  at  $\xi = 0.2$ ,  $Q'^2 = 7 \text{ GeV}^2$ ,  $-t = 0.4 \text{ GeV}^2$  and with  $\theta$  integrated over  $[\pi/4, 3\pi/4]$ . Bottom panel:  $A_{\ell U}$  as a function of  $t$  for  $\phi = 90^\circ$  at  $\xi = 0.2$ ,  $Q'^2 = 7 \text{ GeV}^2$  and  $\theta$  integrated over  $[\pi/4, 3\pi/4]$ .

we noticed earlier, the neutron BH is dominated by the nucleon magnetic form factor contribution which has an opposite sign to the proton electric and magnetic form factors. On the TCS side,  $H^n$  has the same sign than  $H^p$ . The product of the BH and of the TCS processes, and therefore the asymmetry, has thus an opposite sign between the neutron and proton cases when only  $H^n$  is taken into account. In contrast,  $E^n$  has an opposite sign to  $E^p$  and therefore the asymmetry becomes, like for the proton, negative when the GPD  $E^n$  is included. This asymmetry appears therefore rather interesting to study the GPD  $E^n$ .

We recall that the GPD  $E$  is one of the two GPDs entering Ji's sum rule:

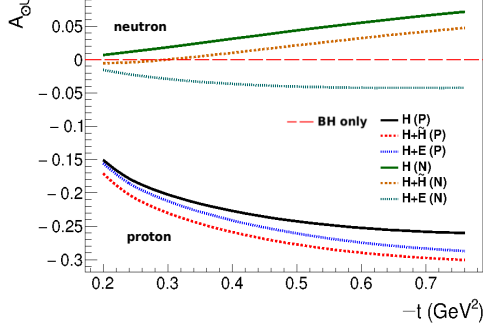


Figure 4:  $A_{\odot U}$ , for the neutron and proton target cases, as a function of  $t$  for  $\phi = 90^\circ$  at  $\xi = 0.2$ ,  $Q'^2 = 7 \text{ GeV}^2$  and  $\theta$  integrated over  $[\pi/4, 3\pi/4]$ .

$$J_q = \frac{1}{2} \int_{-1}^{+1} dx x [H^q(x, \xi, t=0) + E^q(x, \xi, t=0)] , \quad (12)$$

Since  $A_{\odot U}$  on the neutron appears to be mainly governed by the GPD  $E$ , it can be interesting, in the model-dependent framework of VGG that we just described, to calculate  $A_{\odot U}$  directly as a function of  $J^u$  and  $J^d$ . We show in the top left panel of Fig. 5 the results of our calculations for  $A_{\odot U}$  at  $\phi = 90^\circ$ ,  $\xi = 0.2$ ,  $Q'^2 = 7 \text{ GeV}^2$ ,  $-t = 0.4 \text{ GeV}^2$  and  $\theta$  integrated over  $[\pi/4, 3\pi/4]$  for different values of  $J^u$  and  $J^d$ . For the total angular momentum values considered, the figure shows the rather strong sensitivity of the asymmetry which varies from -6% to 13%. In the bottom left panel of Fig. 5, for comparison, we show, in the same VGG framework, the sensitivity of the neutron DVCS beam spin asymmetry  $A_{LU}$  to  $J^u$  and  $J^d$ . One notices as well the sensitivity of this observable to  $J^u$  and  $J^d$  with in particular also changes of sign. However, the amplitudes of the asymmetries for the neutron DVCS case are about a factor of 3 smaller than in the neutron TCS case. We recall that there is an approved experimental proposal with the CLAS detector at JLab to measure the neutron DVCS beam spin asymmetry [22]. Although count rates for TCS can be expected to be less important than for DVCS, the larger TCS asymmetry can possibly provide an interesting alternative way to access the GPD  $E$ .

As a side remark, we note that TCS and DVCS asymmetries have opposite signs w.r.t. each other, i.e. the TCS asymmetry is positive when the DVCS asymmetry is negative and vice-versa. It was indeed shown in Ref. [23] that the TCS amplitude is the conjugate of the

linking the total angular momentum ( $J_q$ ) carried by quarks of flavor  $q$  to the sum of the second moments over  $x$  of the GPDs  $H$  and  $E$ . The GPD  $H$  can be considered as relatively well constrained due to its model-independent relations with parton densities and form factors. This is much less the case for the GPD  $E$  whose forward limit is not constrained at all. The unknown part of  $J_q$  therefore lies essentially in the GPD  $E$ . In the VGG model, the GPD  $E^q$  is parametrized as a function of  $J_q$  which is taken as a free parameter [2]. The idea is that the VGG model assumes a certain shape in  $x$  for the GPD  $E^q$  and then the overall normalization of this function is proportional to  $J^q$ . We refer to Ref. [2] for details. Although this relation between  $E^q$  and  $J^q$  is clearly model-dependent, it yields estimates for  $J^u$  and  $J^d$  which are in agreement with other approaches, such as lattice QCD [21].

DVCS amplitude. The TCS  $A_{\odot U}$  and DVCS  $A_{LU}$  asymmetries being proportional to the imaginary part of the TCS+BH amplitude, this naturally explains this opposite sign.

For completeness, we also show in Fig. 5 the sensitivity of the proton TCS and DVCS beam spin asymmetries to  $J^u$  and  $J^d$ . One sees that there is no change of sign of these asymmetries as a function  $J^u$  and  $J^d$  in contrast to the neutron case. This is because the proton beam spin asymmetries are dominated by the GPD  $H$ . We also remark the relative opposite sign of the TCS and DVCS asymmetries w.r.t. each other, as for the neutron.

We now turn to the target single-spin asymmetries. The asymmetries  $A_{Ux}$ ,  $A_{Uy}$  and  $A_{Uz}$  have respectively a  $\sin \phi$ ,  $\cos \phi$  and  $\sin \phi$ -like shapes. We therefore display in Fig. 6 these three asymmetries for, respectively,  $\phi = 90^\circ$ ,  $\phi = 0^\circ$  and  $\phi = 90^\circ$ , as a function of  $-t$ , at the kinematics  $\xi = 0.2$ ,  $Q'^2 = 7 \text{ GeV}^2$  and  $\theta$  integrated over  $[\pi/4, 3\pi/4]$ . The figure shows both the neutron and proton cases. Like for  $A_{\odot U}$ , these observables are sensitive to the imaginary part of the amplitude and therefore the BH alone asymmetry is zero. We also observe an opposite sign for the two kinds of target when TCS is included due to the different sign of the neutron magnetic form factor compared to the proton. All  $A_{U_i}$ 's are dominated by the GPD  $H^n$ . We however note that  $A_{Ux}$  shows in addition a sensitivity to the GPDs  $E^n$  and  $\bar{H}^n$  for the neutron case. Likewise,  $A_{Uz}$  shows an additional sensitivity to  $E^n$  (while to  $\bar{H}^p$  for the proton case).

### C. Double spin asymmetries

We define the double-spin asymmetries as:

$$A_{(\ell, \odot)i} = \frac{(\sigma^{++} + \sigma^{--}) - (\sigma^{+-} + \sigma^{-+})}{\sigma^{++} + \sigma^{--} + \sigma^{+-} + \sigma^{-+}}, \quad (13)$$

where the first superscript  $\pm$  refers to the polarization nature of the beam ( $\ell$  for a linearly polarized photon

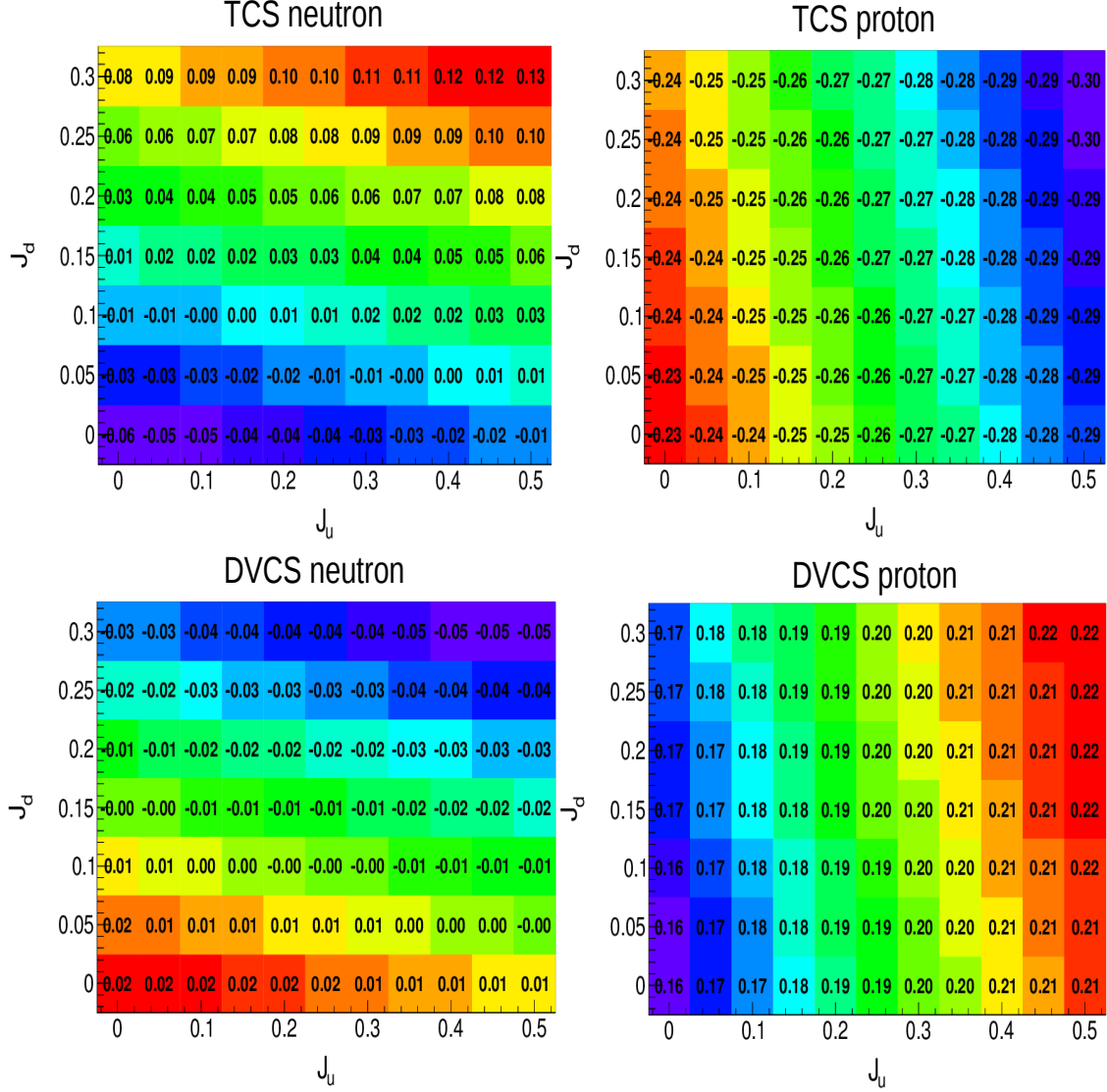


Figure 5: TCS  $A_{\odot U}$  on the neutron (top left panel), TCS  $A_{\odot U}$  on the proton (top right panel), DVCS  $A_{LU}$  on the neutron (bottom left panel), DVCS  $A_{LU}$  on the proton (bottom right panel) as a function of  $J^u$  and  $J^d$ . Calculations are done for  $\phi = 90^\circ$ ,  $\xi = 0.2$ ,  $Q'^2 = 7 \text{ GeV}^2$ ,  $-t = 0.4 \text{ GeV}^2$  and  $\theta$  integrated over  $[\pi/4, 3\pi/4]$ .

beam and  $\odot$  for a circularly polarized photon beam) and the second one to the target's along the axis  $i = x, y, z$ .

In Fig. 7, we show the  $t$ -dependence of the three double spin asymmetries  $A_{\ell x}$ ,  $A_{\ell y}$  and  $A_{\ell z}$  obtained with a linearly polarized photon beam and a polarized target for the neutron and proton target cases. Like for the proton target case [1], the asymmetries have respectively a  $\sin 2\phi$ ,  $\cos 2\phi$  and  $\sin 2\phi$ -like shape. We therefore plot in Fig. 7  $A_{\ell x}$ ,  $A_{\ell y}$  and  $A_{\ell z}$  at  $\phi = 90^\circ$ ,  $\phi = 0^\circ$  and  $\phi = 90^\circ$

respectively, for our typical kinematics  $\xi = 0.2$ ,  $Q'^2 = 7 \text{ GeV}^2$ ,  $-t = 0.4 \text{ GeV}^2$  and  $\theta$  integrated over  $[\pi/4, 3\pi/4]$ . This double-spin asymmetry is sensitive to the imaginary part of the amplitude and therefore the BH alone does not produce any signal. As expected, the sign is opposite for the neutron and proton target cases. We note, for the neutron target case, the particular sensitivity of  $A_{\ell x}$  to the GPDs  $H^n$ ,  $\tilde{H}^n$  and  $E^n$  and of  $A_{\ell z}$  to the GPDs  $H^n$  and  $E^n$ .

In Fig. 8, we show the  $\phi$ -dependence of the three double-spin asymmetries  $A_{\odot x}$ ,  $A_{\odot y}$  and  $A_{\odot z}$  obtained with a circularly polarized photon beam and a polarized target for the  $\gamma n \rightarrow n'e^+e^-$  process. The kinematics

is as before:  $\xi = 0.2$ ,  $Q'^2 = 7 \text{ GeV}^2$ ,  $-t = 0.4 \text{ GeV}^2$  and  $\theta$  has been integrated over  $[\pi/4, 3\pi/4]$ . We show here the  $\phi$ -dependencies as they can be quite intricate and disparate. This double spin asymmetry is sensitive



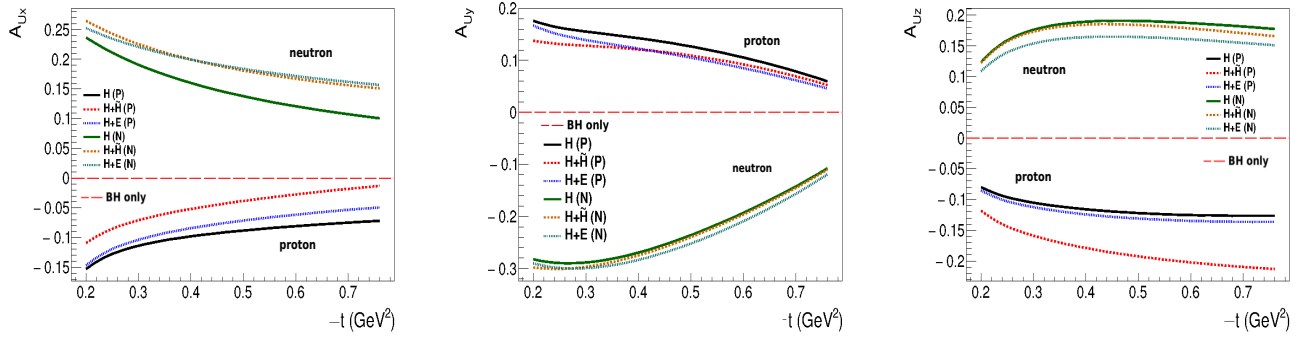


Figure 6: The  $A_{Ux}$  (left panel),  $A_{Uy}$  (central panel) and  $A_{Uz}$  (right panel) asymmetries, as a function of  $t$ , respectively for  $\phi = 90^\circ$ ,  $\phi = 0^\circ$  and  $\phi = 90^\circ$  at  $\xi = 0.2$ ,  $Q'^2 = 7 \text{ GeV}^2$ ,  $-t = 0.4 \text{ GeV}^2$  and for  $\theta$  integrated over  $[\pi/4, 3\pi/4]$ . The results are shown for the neutron and proton target cases.

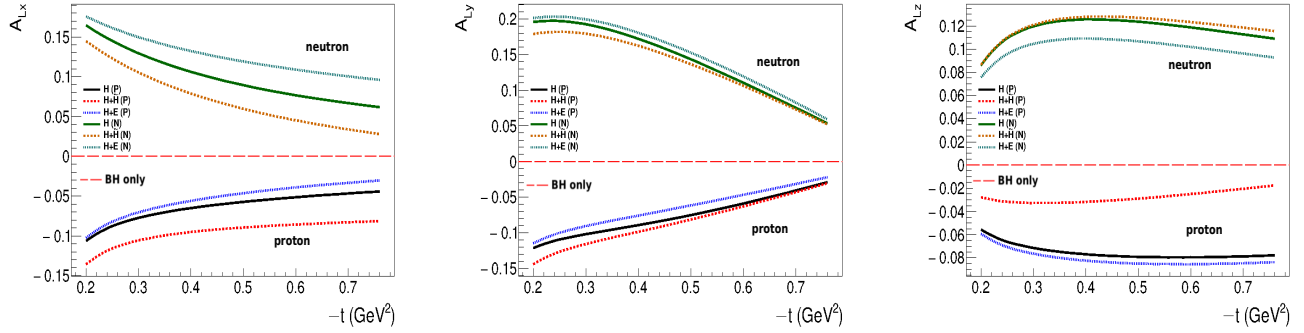


Figure 7: The double-spin asymmetries  $A_{Lx}$  (left panel),  $A_{Ly}$  (central panel) and  $A_{Lz}$  (right panel), respectively for  $\phi = 90^\circ$ ,  $\phi = 0^\circ$  and  $\phi = 90^\circ$ , as a function of  $-t$  for  $\xi = 0.2$ ,  $Q'^2 = 7 \text{ GeV}^2$  and for  $\theta$  integrated over  $[\pi/4, 3\pi/4]$ . The results are shown for the neutron and proton target cases.

to the real part of the amplitude and therefore the BH alone can produce a strong signal by itself. The TCS can change significantly and in various ways the asymmetries w.r.t. BH alone, making this observable very sensitive to various GPD contributions. In particular, one notes the sensitivity to  $\tilde{E}^n$ . The most important TCS influence ap-

pears in  $A_{\odot y}$  where the asymmetry amplitude can change from only a few percent for BH alone to about 30% for a particular GPD configuration.

We finally show in Fig. 9 the  $t$ -dependence of  $A_{\odot x}$ ,  $A_{\odot y}$  and  $A_{\odot z}$  at  $\phi = 90^\circ$ ,  $\phi = 0^\circ$  and  $\phi = 90^\circ$  respectively, for the neutron and proton target cases.

#### IV. CONCLUSIONS

In summary, we have presented a first phenomenological study of the  $\gamma n \rightarrow n'e^+e^-$  reaction in the handbag approach. Using the GPDs from the VGG model, we calculated the unpolarized cross section and all the beam and target single and double spin asymmetries of the pro-

cess for typical kinematics of JLab at 12 GeV. We showed the sensitivities of these observables to various GPDs. In particular, we highlighted the sensitivity of the circularly polarized beam spin asymmetry to the elusive GPD  $E$  (of the neutron), which is of special interest for the study of the nucleon spin decomposition.

The cross section of the  $\gamma n \rightarrow n'e^+e^-$  process is only a

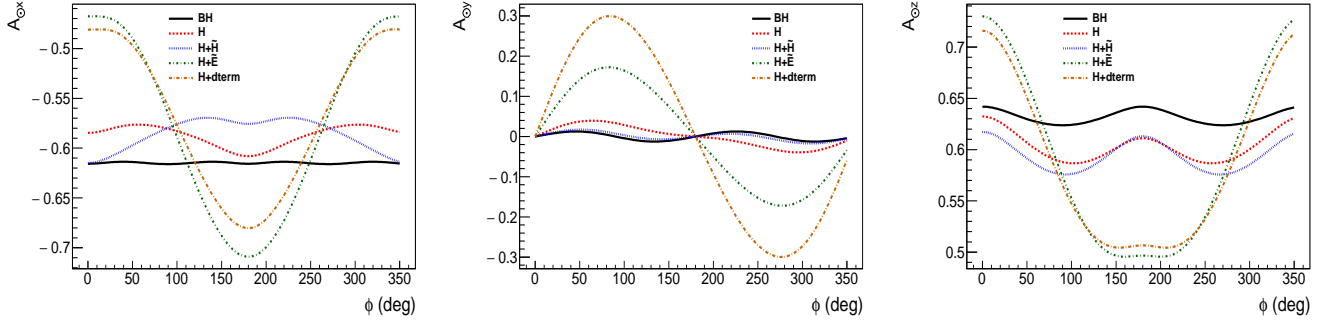


Figure 8: The double-spin asymmetries  $A_{\odot x}$  (left panel),  $A_{\odot y}$  (central panel) and  $A_{\odot z}$  (right panel) as a function of  $\phi$  for  $\xi = 0.2$ ,  $Q'^2 = 7 \text{ GeV}^2$ ,  $-t = 0.4 \text{ GeV}^2$  and for  $\theta$  integrated over  $[\pi/4, 3\pi/4]$ .

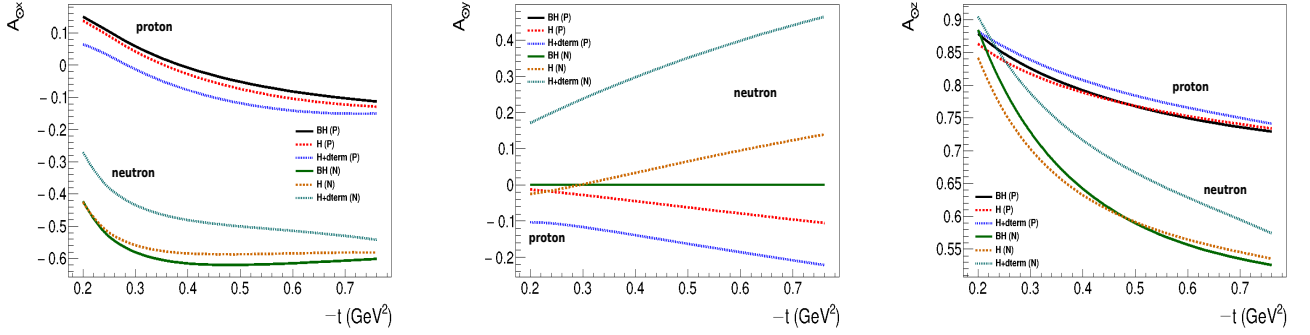


Figure 9: The  $A_{\odot x}$  (left panel),  $A_{\odot y}$  (central panel) and  $A_{\odot z}$  (right panel) asymmetries, respectively for  $\phi = 0^\circ$ ,  $\phi = 90^\circ$  and  $\phi = 0^\circ$ , as a function of  $t$  for  $\xi = 0.2$ ,  $Q'^2 = 7 \text{ GeV}^2$ ,  $-t = 0.4 \text{ GeV}^2$  and for  $\theta$  integrated over  $[\pi/4, 3\pi/4]$ . Calculations are done for the neutron and proton target cases.

factor 2 below the  $\gamma p \rightarrow p' e^+ e^-$ , for which experimental proposals have been approved at JLab, and some asymmetries are sizeable, even more than for the proton in some cases. Thus, the study of TCS on the neutron appears feasible experimentally and promises to bring new important constraints on GPD physics, in particular on the GPD  $E^n$  and, more generally, the flavor separation of GPDs.

### Acknowledgments

The work of M.V. is supported by the Deutsche Forschungsgemeinschaft DFG through the Collaborative

Research Center “The Low-Energy Frontier of the Standard Model” (SFB 1044) and the Cluster of Excellence “Precision Physics, Fundamental Interactions and Structure of Matter” (PRISMA). M. G. and M. V. are also supported by the Joint Research Activity “GPDex” of the European program Hadron Physics 3 under the Seventh Framework Programme of the European Community. M.B. and M.G. also benefitted from the GDR 3034 “PH-QCD” and the ANR-12-MONU-0 008-01 “PARTONS” support.

[1] M. Boër, M. Guidal and M. Vanderhaeghen, Eur. Phys. J. A **51**, 103 (2015).

[2] K. Goeke K, M.V. Polyakov and M. Vanderhaeghen,



- Prog. Part. Nucl. Phys. **47**, 401 (2001).
- [3] M. Diehl, Phys. Rept. **388**, 41 (2003).
  - [4] A.V. Belitsky and A.V. Radyushki, Phys. Rept. **418**, 1 (2005).
  - [5] M. Guidal, H. Moutarde and M. Vanderhaeghen, Rept. Prog. Phys. **76**, 066202 (2013).
  - [6] S. Boffi and B. Pasquini, Riv. Nuovo Cim. **30**, 387 (2007).
  - [7] M. Guidal, M. V. Polyakov, A. V. Radyushkin and M. Vanderhaeghen, Phys. Rev. D **72**, 054013 (2005).
  - [8] D. Mueller, D. Robaschik, B. Geyer, F. M. Dittes and J. Horejsi, Fortsch. Phys. **42**, 101 (1994).
  - [9] A.V. Radyushkin, Phys.Lett.B **380**, 417 (1996).
  - [10] X. Ji, Phys.Rev.Lett. **78**, 610 (1997).
  - [11] X. Ji, Phys.Rev.D **55**, 7114 (1997).
  - [12] M. Vanderhaeghen, P.A.M. Guichon and M. Guidal, Phys. Rev. Lett. **80**, 5064 (1998).
  - [13] M. Vanderhaeghen, P. A. M. Guichon and M. Guidal, Phys. Rev. D **60**, 094017 (1999).
  - [14] A. V. Radyushkin, Phys. Rev. D **59**, 014030 (1999).
  - [15] A. V. Radyushkin, Phys. Lett. B **449**, 81 (1999).
  - [16] M. V. Polyakov and C. Weiss Phys. Rev. D **60**, 114017 (1999).
  - [17] G. Warren *et al.* [Jefferson Lab E93-026 Collaboration], Phys. Rev. Lett. **92**, 042301 (2004).
  - [18] G. Kubon, H. Anklin, P. Bartsch, D. Baumann, W. U. Boeglin, K. Bohinc, R. Bohm and M. O. Distler *et al.*, Phys. Lett. B **524**, 26 (2002).
  - [19] I. Albayrak *et al.*, CLAS Collaboration, Jefferson Lab PAC 39 Proposal, *Timelike Compton Scattering and  $J/\Psi$  photoproduction on the proton in  $e^+e^-$  pair production with CLAS12 at 11 GeV*  
[https://www.jlab.org/exp\\_prog/proposals/12/PR12-12-001.pdf](https://www.jlab.org/exp_prog/proposals/12/PR12-12-001.pdf)
  - [20] E. Pasyuk [CLAS Collaboration], Chin. Phys. C **33**, 1205 (2009)
  - [21] C. Alexandrou, EPJ Web Conf. **73**, 01013 (2014).
  - [22] S. Niccolai *et al.*, CLAS collaboration, Jefferson Lab PAC 37 proposal, *Deeply Virtual Compton Scattering on the neutron with CLAS12 at 11 GeV*.  
[https://www.jlab.org/exp\\_prog/proposals/11/PR12-11-003.pdf](https://www.jlab.org/exp_prog/proposals/11/PR12-11-003.pdf)
  - [23] D. Mueller, B. Pire, L. Szymanowski and J. Wagner, Phys. Rev. D **86**, 031502 (2012).